

Symmetry Locking and Commensurate Vortex Domain Formation in Periodic Pinning Arrays

A.N. Grigorenko[†], S.J. Bending,

Department of Physics, University of Bath, Claverton Down, Bath, BA2 7AY, UK

M.J. Van Bael, M. Lange, V.V. Moshchalkov,

Laboratorium voor Vaste-Stoffysica en Magnetisme, Katholieke Universiteit Leuven, Celestijnenlaan 200D, 3001 Leuven, Belgium

H. Fangohr, P.A.J. de Groot

School of Engineering Sciences & Department of Physics and Astronomy, University of Southampton, Southampton, SO17 1BJ, UK

Abstract

The spontaneous formation of *domains* of commensurate vortex patterns near rational fractional matching fields of a periodic pinning array has been investigated with high resolution scanning Hall probe microscopy. We show that domain formation is promoted due to the efficient incorporation of mismatched excess vortices/vacancies at the *corners* of domain walls, which outweighs the high energetic cost of creating them. Molecular dynamics simulations with a generic pinning potential reveal that domains are only formed when the vortex-vortex interactions are long range. In the multi-domain regime magnetisation data near rational fractional matching fields clearly support this mechanism of the nucleation and propagation of domain walls.

PACS numbers: 74.60.Ge, 74.25.Ha, 74.76.Db

In many physical systems high symmetry ordering only occurs for certain specific values of the system parameters. These transient symmetries are important for the excitation spectrum of the system and often appear in atomic solids, liquid crystals as well as magnetic materials. A technologically important example is a superconductor containing a periodic artificial pinning array, a system which has been extensively investigated in recent years with a view to enhancing the superconducting critical current. In this case the problem is that of filling the ordered array with vortices, and commensurate structures can be formed at certain specific values of the vortex density when sharp peaks in the bulk magnetisation and critical current have been observed [1-7]. Commensurate structures have been directly imaged on the microscopic scale using Lorentz [8] and scanning Hall probe (SHPM) [9,10] microscopies. From a theoretical point of view the probability of observing these "pure" matching structures on a macroscopic scale is proportional to the measure of the parameter space at which they exist and, strictly speaking, is supposed to be zero when interactions can be neglected. This constraint is, however, relaxed for integer matching fields (when an integer number of flux quanta per unit cell are applied) due to magnetic 'lock-in' phenomena whereby the local magnetic induction becomes fixed at the matching field over a finite applied field range. Strong integer matching effects arise due to the formation of a special critical state for which two possible models have been proposed. The first is a multi-terrace state whereby a staircase of terraces of different integer matching fields exists with very high screening currents flowing at the inter-terrace boundaries [11]. Alternatively, close to T_c a single integer terrace may exist with strong screening currents flowing at the sample edges [12]. Weaker matching effects are observed near rational fractional matching fields, where molecular dynamics simulations predicted [13] and imaging experiments confirmed [8], that ordered vortex structures form which are commensurate with the pinning array. Magnetic lock-in phenomena appear to be very weak at rational fractional matching yet magnetisation

measurements reveal that commensurate configurations still occur within a small field range. One important feature that distinguishes fractional matching states from integer ones is that two or more possible degenerate structures always exist under the symmetry transformations of the pinning array. Recent SHPM images have revealed the spontaneous formation of complex composite structures of degenerate domains separated by domain walls near rational fractional filling [9,10]. This phenomenon was entirely unanticipated since, in stark contrast to ferromagnetic materials, the energies and magnetisation of different domains are identical, and the driving force for domain formation and the estimation of typical domain sizes has, until now, remained an unsolved problem. Here we show that domain formation is a direct consequence of long-range vortex-vortex interactions which exist in thin superconducting films. *Under these conditions corners in domain walls prove to be efficient ‘sinks’ for unmatched excess vortices or vacancies, and allow commensurate states to exist over a broad range of applied magnetic fields.*

A variety of different artificial pinning strategies have been successfully employed including arrays of sub-micron holes (antidots) [1-3] or ferromagnetic dots with both in-plane [4,5] and perpendicular anisotropy [6,7], and the qualitative features of both integer and fractional matching phenomena appear to be generic to all of these. Our imaging experiments were performed on a 50nm granular Pb film ($T_c = 7.17$ K) deposited over an $a=1\mu\text{m}$ period square array ($H_1 = \Phi_0 / a^2 = 20.67\text{Oe}$) of $0.4\mu\text{m}$ square ferromagnetic ‘dots’ with perpendicular magnetic anisotropy patterned in a $[\text{Co}(0.3\text{ nm})/\text{Pt}(1.1\text{ nm})]_{10}$ multilayer film. The overall array size was $\sim 2\text{mm} \times 2\text{mm}$ (much bigger than any important lengthscale) and contained about 4×10^6 magnetic dots. It exhibited rather square magnetisation loops with large coercive fields ($\sim 1\text{kOe}$) allowing the generation of imposed magnetic templates which are stable at the much lower applied fields where matching effects are observed. A schematic diagram of three periods of the investigated sample is shown in the inset to Fig.1 and further

details of the sample preparation are given elsewhere [5,7,16]. The effective penetration depth of our Pb film (thickness $t=50\text{nm}$) at high temperatures when $\lambda(T)\gg t$ [14] was estimated from the upper critical field $H_{c2}(0)$ measured on a 25 nm reference Pb, film and found to be $\Lambda(T) = 2\lambda^2(T)/t = 92 \text{ nm}/(1-T/T_c)$. The SHPM used was able to generate maps of the local induction with $\sim 0.4 \mu\text{m}$ spatial resolution and minimum detectable fields $\sim 1\mu\text{T}/\text{Hz}^{0.5}$. A more detailed description is given in ref. [15].

Fig. 1(a) shows a ‘local’ magnetisation loop ($M_\ell = B_\ell - \mu_0 H$) measured a few microns above the surface of our sample, with the stationary Hall probe at a temperature of 6.9K ($T/T_c=0.962$), after the pinning array had been magnetised to saturation in the down ($H<0$) direction above T_c . Strongly asymmetric vortex pinning is observed with the magnetisation collapsing almost to zero for $H>0$, which is reported elsewhere [16]. With the applied field parallel to the magnetisation of the Co/Pt dots ($H<0$) clear matching peaks are seen at integer ($-1.H_1, -2.H_1$) and rational fractional ($-3/4.H_1, -3/2.H_1$) matching fields. Surprisingly no clearly resolved structure is seen near $-1/2.H_1$ or $-1/3.H_1$ although, as we will show, commensurate structures definitely exist at these matching fields. Indeed the magnetisation is remarkably smooth and featureless for $-0.75.H_1<H<-0.2H_1$. The parallel plot of local magnetic induction (Fig. 1(b)) reveals lock-in phenomena at integer matching fields and $H=-3/4.H_1$ where the slope becomes much shallower. However, there is again no clear evidence for lock-in at other rational fractions.

High-resolution SHPM images were made of the vortex structures formed after field-cooling to low temperatures. Fig. 2(a)-(e) shows a typical family of images at fields close to $-H_1/2$. At exactly $H=-H_1/2$ (Fig. 2(d)) a very well ordered ‘checkerboard’ structure is observed where every second pinning site is occupied by a vortex. Remarkably, cooling the sample at fields slightly above/below $-H_1/2$ did not result in excess vortices/vacancies in the commensurate lattice as is the case at field values close to integer matching. Instead

coexisting domains of the two degenerate commensurate states (related by a translation of one lattice vector of the pinning array) are observed separated by domain walls of varying complexity. The domain walls appear to move smoothly as slightly different cooling fields are employed (e.g. the transition from Fig. 2(b) to Fig. 2(c)) and their presence does not seem to be related to the possible existence of inhomogeneities in the pinning array. There is a crucial difference between domain structures at fields slightly above and slightly below half-matching. For $|H| < H_1/2$, when vacancies should exist in the checkerboard structure, the corners where domain walls bend by 90° comprise a ‘low density’ square cluster of *three unoccupied pins and one occupied one*. In contrast, for $|H| > H_1/2$, when excess vortices should exist, the corners are composed of a ‘high density’ cluster of *three occupied pins and one unoccupied one*. Hence, despite the increase in energy associated with the straight segments of domain wall, domain formation is favoured because the incorporation of the mismatched vortices/vacancies into domain wall corners lowers the overall energy. *This represents an elegant solution to the matching problem as each domain is commensurate with the pinning array yet the mean induction averaged over several domains can vary about $-\mu_0 H_1/2$.*

For a short-range vortex-vortex interaction one would expect the energy of the straight domain walls to be prohibitively large and the ground state should consist of ‘checkerboard-interstitials’ or on-site ‘vacancies’. However, in thin films at temperatures close to T_c , when $\lambda(T) \gg t$, Pearl [14] has shown that vortex-vortex interactions are long range, decaying as $\log_e(r)$ for $r \ll \Lambda(T)$ and $1/r$ for $r \gg \Lambda(T)$, and domains can become favourable. Figs. 3(a)-(c) illustrate some possible domain structures. Simple “bookkeeping” reveals that the square domain in Fig. 3(a) with four high density corners can accommodate exactly one excess vortex. Translating the square domain one lattice site vertically (or horizontally) as shown in Fig. 3(b) generates low density corners which can accommodate

exactly one vacancy. Alternatively stripe-like domains could form as illustrated in Fig. 3(c) with either high- or low-density domain wall corners. The image shown in Fig. 2(a) is strongly suggestive of the existence of such stripe domains which also represent an efficient way for the domain wall to move by means of successive jumps of the vortex situated near the domain wall step.

Molecular dynamics simulations were performed with a generic pinning potential to demonstrate that long-range vortex-vortex interactions promote domain formation. Considering vortices as stiff massless lines, overdamped Langevin dynamics simulations of an effectively two-dimensional vortex system were carried out (more details are given in [17]). The long-range vortex-vortex interaction energy ($\lambda(T) \gg t$) was described by [14]

$$U^{vv}(\mathbf{r}) = \frac{2\Phi_0^2 t}{4\pi\mu_0\lambda(T)^2} \left(H_0\left(\frac{r}{\Lambda}\right) - Y_0\left(\frac{r}{\Lambda}\right) \right), \quad (1)$$

where $H_0(Y_0)$ is a Struve(Bessel) function of the second kind. The short-range vortex-vortex interaction energy which is appropriate in thick films ($t \gg \lambda(T)$) was described by

$$U^{vv}(\mathbf{r}) = \frac{2\Phi_0^2 t}{4\pi\mu_0\lambda(T)^2} K_0\left(\frac{r}{\lambda}\right), \quad (2)$$

where K_0 is the modified Bessel function of the second kind.

Periodic boundary conditions were employed and the differential equation solved numerically in order to compute the time progression of the system. Starting from a high temperature molten vortex configuration, we slowly annealed the system in the presence of a periodic pinning potential ($a=1\mu\text{m}$) representing the square array of magnetic dots, to zero temperature. The interaction of a vortex with each pinning site was assumed proportional to $\frac{-1}{(\rho^2 + c)}$ where ρ was the distance to the center of the pin, and c^{-1} a measure of the pin's depth. The results of the model did not depend sensitively on the details of the pinning

potential. Figs. 3(d)-(e) show typical results of the simulation for 400 pinning sites when the long-range interaction (eqn. (1)) with $\Lambda=2\mu\text{m}$ was used in order to compare with the data of Fig. 1. For exactly half-matching conditions the checkerboard structure of Fig. 3(e) is reproduced. With one vacancy present, a rectangular domain with four low-density corners is created (Fig. 3(d)), while with one excess vortex a square domain with four high-density corners is found (Fig. 3(f)), in agreement with the images in Fig. 2. Fig. 3(g) is a repeat of the calculation with one excess vortex for the short-range vortex-vortex potential (eqn. (2)) where we find, as expected, that the excess vortex is located at an unoccupied pin in the checkerboard lattice. We find that the effective penetration depth $\Lambda(T)$, which diverges quite rapidly near T_c , sets a characteristic lengthscale for the size of the domains. The effective penetration length used in simulations $\Lambda=2\mu\text{m}$ ($T/T_c=0.954$) represents a much higher reduced temperature than that corresponding to our field-cooled SHPM images. We assume, however, that the latter represent metastable states which become ‘frozen in’ close to T_c where the penetration depth is much longer.

The checkerboard structure at $|H|=H_1/2$ preserves the four-fold rotational symmetry of the pinning array and appears rather robust with respect to the specific form of vortex-vortex interactions. This is not true of the structure at $|H|=H_1/3$ where the ground state was originally predicted to be one of six degenerate symmetry-breaking chain states as sketched in Fig. 4(a) [18]. These represent an inefficient way of packing vortices and one might anticipate that a multi-domain state would have lower energy, even *exactly* at the matching field [19]. The multi-domain SHPM image at $H = -H_1/3$ (Fig. 4(b)) shows this to be the case. This behaviour is also confirmed in the simulation with the same long-range vortex-vortex potential as before. A typical simulation for 24×24 sites is illustrated in Fig. 4(d) and is a complex composite of all six degenerate chain structures (a few possible domain identifications have been sketched near the center).

In conclusion, we have shown that vortex configurations of an ordered pinning array consist of coexisting ordered domains separated by domain walls over a range of fields near rational fractional matching. Domain formation is a consequence of long-range vortex-vortex interactions in thin films at high temperatures and lowers the overall energy because the *domain corners incorporate excess vortices*. By this subtle means the system is able to lock to the symmetry of the pinning array within a domain, yet the magnetic induction averaged over several domains can vary around the matching field. Matching structures, which strongly break the symmetry of the pinning array, can be unstable with respect to domain formation, even *exactly* at the matching field. The number of domains and domain sizes are generally governed by the effective penetration depth (at which the domain structure becomes frozen), the lattice spacing and the number of mismatched vortices. In the multi-domain regime magnetisation data near rational fractional matching fields should be interpreted in terms of the nucleation and propagation of domain walls rather than a single- or multiple-terrace critical state.

This work was supported in the UK by EPSRC and MOD Grant No. GR/L96448. The authors thank S. Raedts, L. Van Look, K. Temst, J. Bekaert and R. Jonckheere for help with sample preparation and C.J. Olson and C. Reichhardt for valuable discussions. This work was supported by the Belgian Inter-University Attraction Poles (IUAP) and Flemish Concerted Research Actions (GOA) programs, by the ESF "VORTEX" program and by the Fund for Scientific Research-Flanders (FWO). MJVB is a Postdoctoral Research Fellow of the FWO.

[†]*Current address:* Department of Communication and Electronic Engineering, University of Plymouth, Drake Circus, Plymouth, PL4 8AA, United Kingdom

References

- [1] A.F. Hebard, A.T. Fiory, and S. Somekh, *Appl. Phys. Lett.* **32**, 73 (1978).
- [2] M. Baert *et al.*, *Phys. Rev. Lett.* **74**, 3269 (1995).
- [3] M. Baert *et al.*, *Europhys. Lett.* **29**, 157 (1995).
- [4] J.I. Martín *et al.*, *Phys. Rev. Lett.* **79**, 1929 (1997).
- [5] M.J. Van Bael *et al.*, *Phys. Rev. Lett.* **86**, 155 (2001).
- [6] D.J. Morgan and J.B. Ketterson, *Phys. Rev. Lett.* **80**, 3614 (1998).
- [7] M.J. Van Bael *et al.*, *Physica C* **369**, 97 (2002).
- [8] K. Harada *et al.*, *Science* **274**, 1167 (1996).
- [9] S.B. Field *et al.*, *Phys. Rev. Lett.* **88**, 067003 (2002).
- [10] A.N. Grigorenko *et al.*, *Phys. Rev. B.* **63**, 052504 (2001).
- [11] L.D. Cooley and A.M. Grishin, *Phys. Rev. Lett.* **74**, 2788 (1995).
- [12] V.V. Moshchalkov *et al.*, *Phys. Rev. B* **54**, 7385 (1996).
- [13] C. Reichhardt *et al.*, *Phys. Rev. B* **54**, 16108 (1996).
- [14] J. Pearl, *Appl. Phys. Lett.* **5**, 65 (1964).
- [15] A. Oral, S.J. Bending and M. Henini, *Appl. Phys. Lett.* **69**, 1324 (1996).
- [16] M.J. Van Bael *et al.* (submitted).
- [17] H. Fangohr, S. J. Cox and P. A. J. de Groot, *Phys. Rev. B.* **64**, 064505. (2001).
- [18] G.I. Watson, *Physica (Amsterdam)* **246A**, 253 (1997).
- [19] C. Reichhardt, N. Gronbech-Jensen, *Phys. Rev. B* **63**, 054510 (2001).

Figure Captions

Fig. 1 Local magnetisation (top) and magnetic induction (bottom) as a function of applied magnetic field at 6.9 K. Dashed lines indicate the expected location of matching features. Inset shows a schematic diagram of the pinning array.

Fig. 2. SHPM images of commensurate vortex configurations after field-cooling close to the half-matching field. (a) $H = -0.984.H_1/2$, $T=5.5K$ (grayscale (GS) spans $\sim 0.28mT$) (b) $H = -0.997.H_1/2$, $T=5.5K$ (GS $\sim 0.24mT$, (c) $H = -0.990.H_1/2$, $T=5.5K$ (GS $\sim 0.27mT$), (d) the ‘checkerboard’ configuration at $H = -H_1/2$, $T=6.8K$ (GS $\sim 0.20mT$), (e) $H = -1.04.H_1/2$, $T=6.0K$ (GS $\sim 0.20mT$). The right-hand panels show clearer sketches of the domain structure in each adjacent image.

Fig. 3 Sketches of possible domain structures. Square domain accommodating (a) one excess vortex and (b) one vacancy. (c) Possible stripe domain structure. Molecular dynamics simulation results with a long-range vortex-vortex interaction for (d) half-matching field plus one vacancy, (e) half-matching field and (f) half-matching field plus one excess vortex. (g) Same simulation as (f) but with a short-range vortex-vortex interaction.

Fig. 4 (a) Sketch of expected commensurate structure at one-third matching. (b) SHPM image of commensurate vortex domains after field-cooling at $H = -H_1/3$, $T=5.5K$ (GS $\sim 0.26mT$). (c) Clearer sketch of the domain structure in (b). (d) Molecular dynamics simulation result with a long-range vortex-vortex interaction for $H = -H_1/3$.

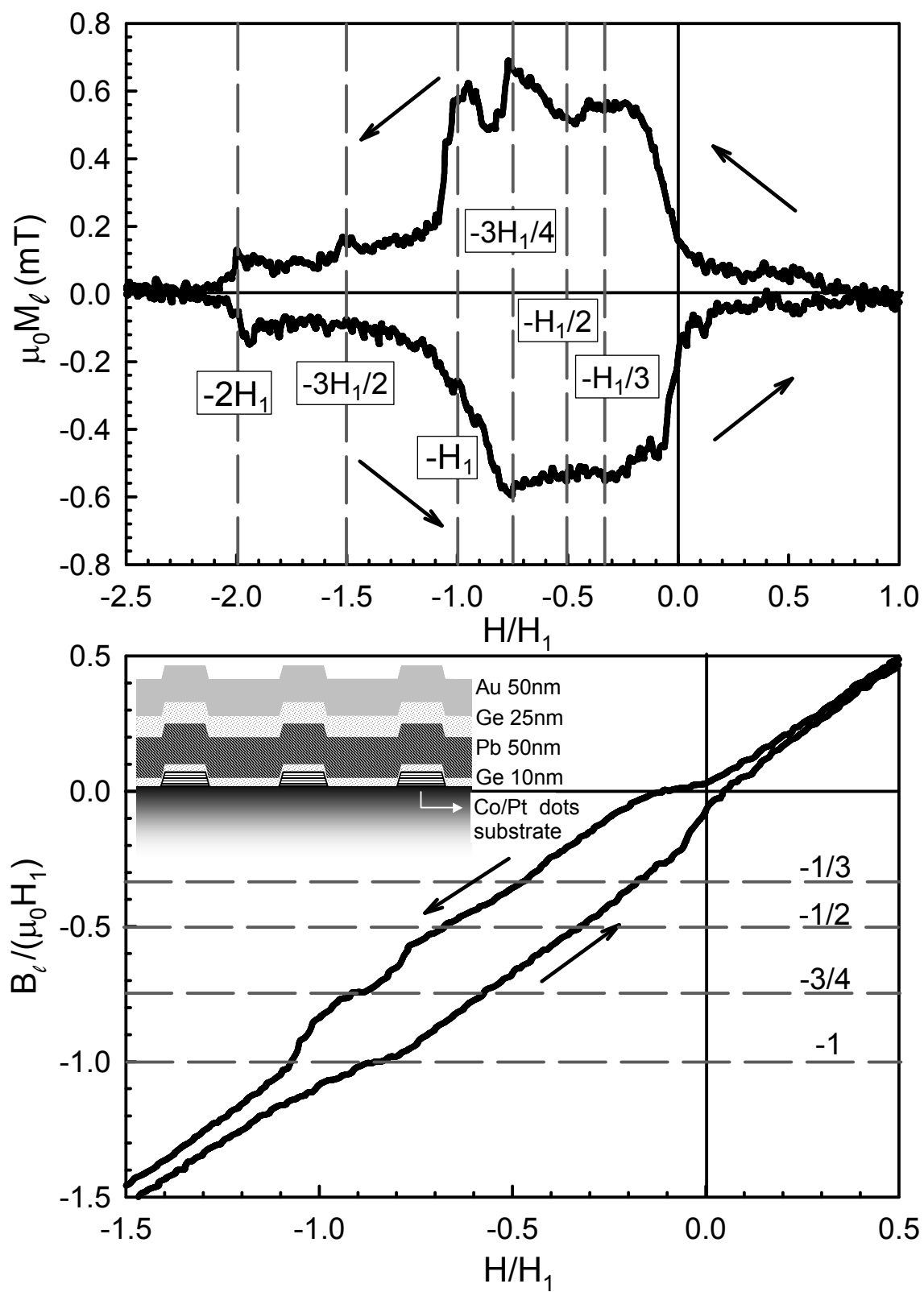


Fig. 1 ‘Symmetry Locking and Commensurate Vortex Domain...’, A.N.Grigorenko *et al.*

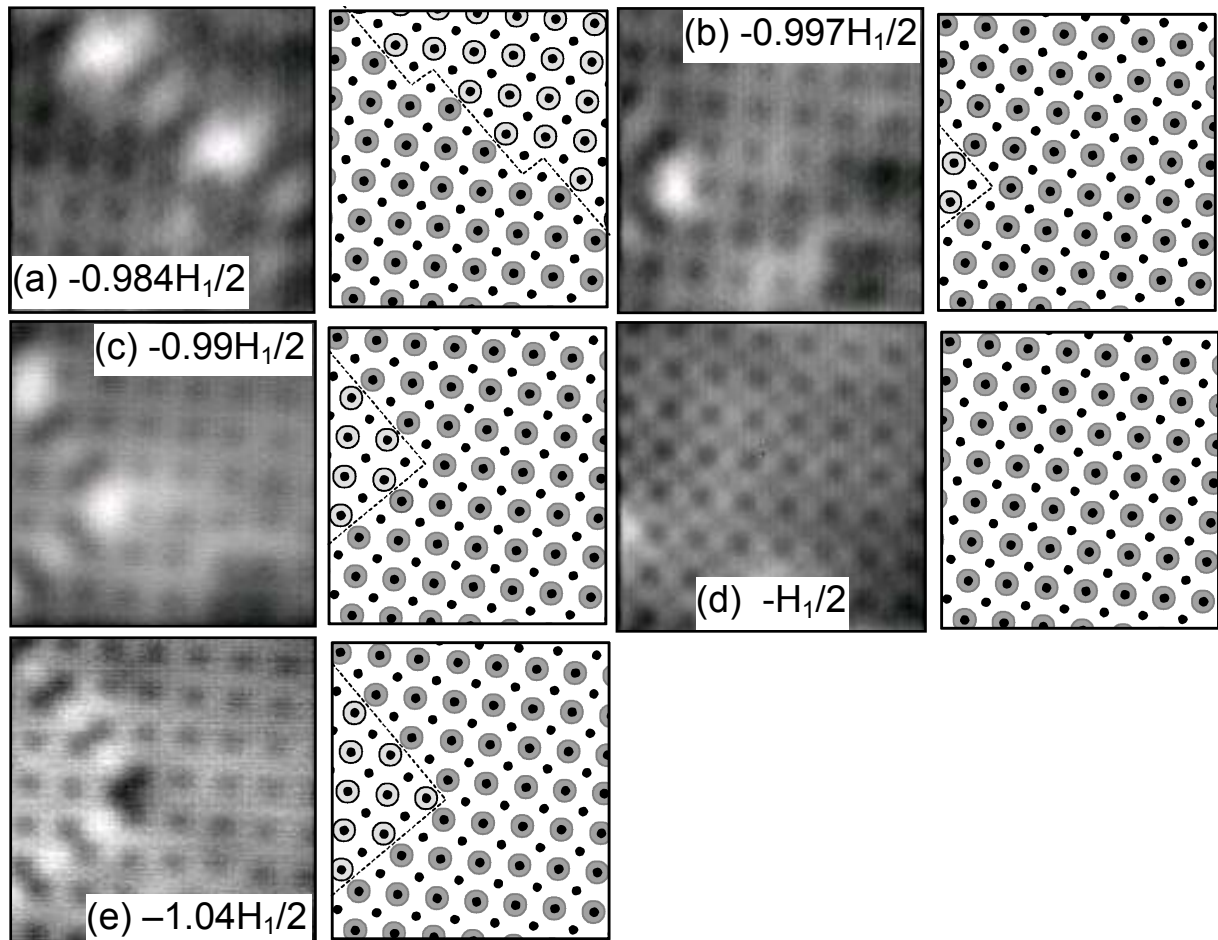


Fig. 2 'Symmetry Locking and Commensurate Vortex Domain...', A.N.Grigorenko *et al.*

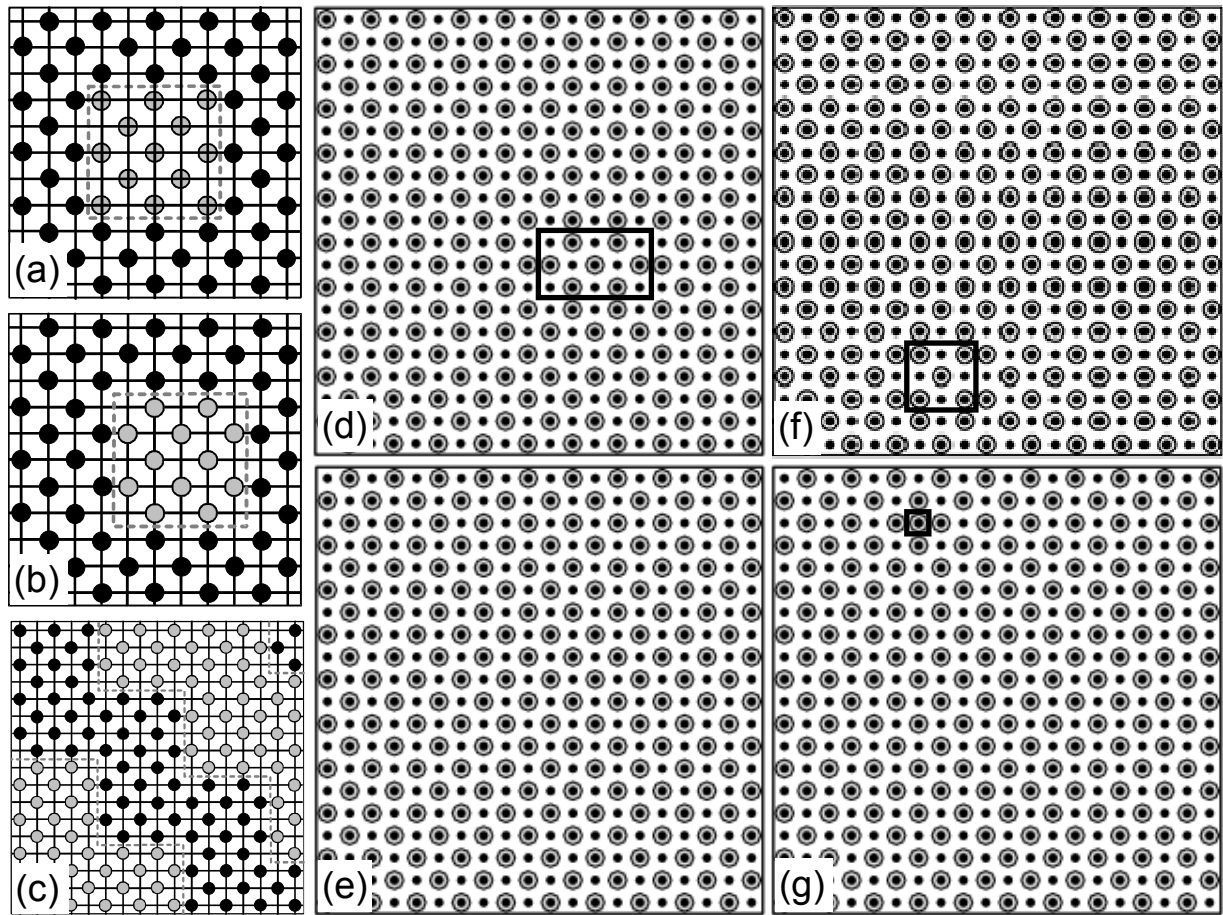


Fig. 3 ‘Symmetry Locking and Commensurate Vortex Domain...’, A.N.Grigorenko *et al.*

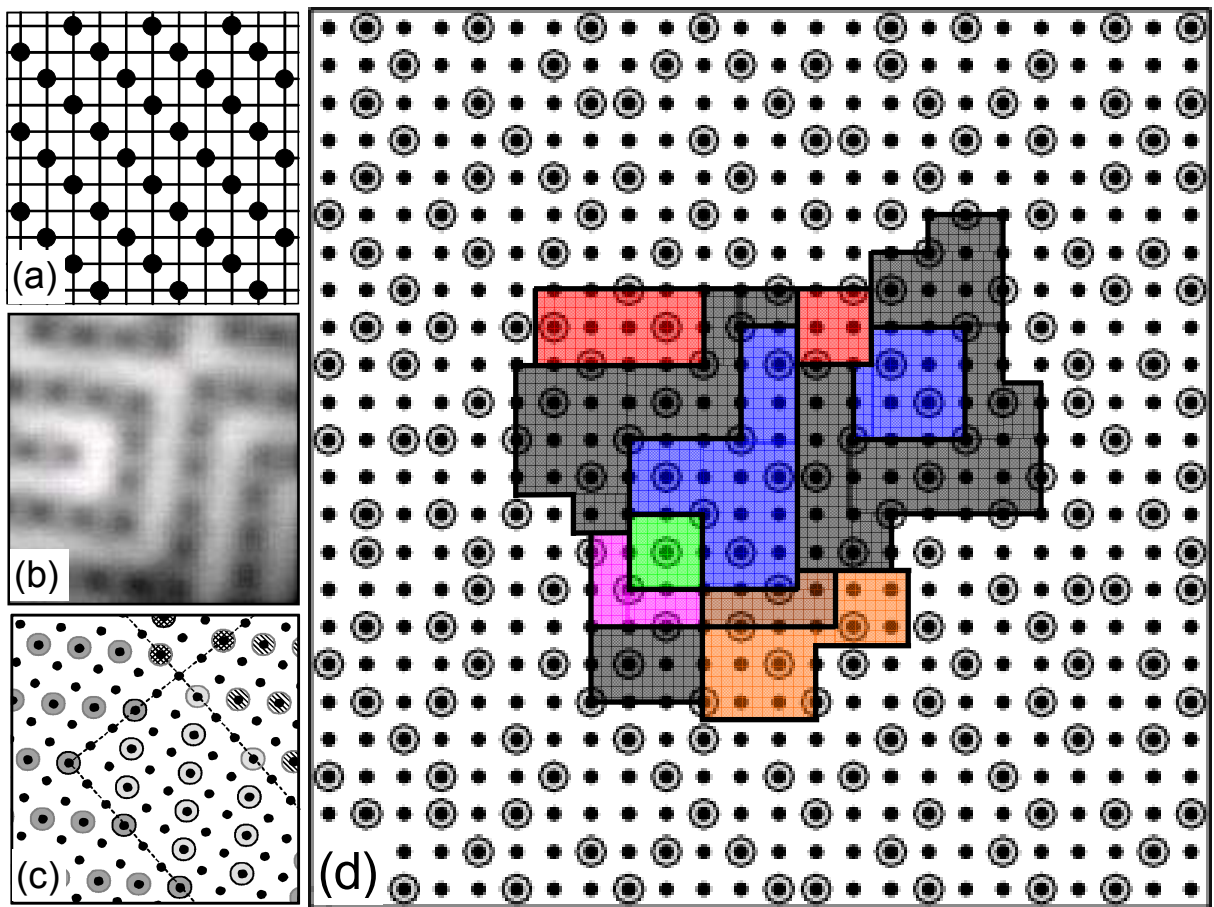


Fig. 4 ‘Symmetry Locking and Commensurate Vortex Domain...’, A.N.Grigorenko *et al.*